JOURNAL OF APPLIED POLYMER SCIENCE VOL. 18, PP. 1753–1772 (1974)

Molecular Orientation in Injection Molding

Z. TADMOR,* *Rheology Research Center and Chemical Engineering Department, University of Wisconsin, Madison, Wisconsin 53706*

Synopsis

A semiquantitative model is proposed to explain the complex molecular orientation distribution, observed in injection moldings of amorphous polymers. The model incorporates flow and heat transfer mechanisms coupled with molecular theories. The orientation in the surface skin is related to steady elongational flow in the advancing front, whereas the orientation in the core is related to the shear flow, behind the front, between two solidyfying layers. Coupled with the elongational and shear-induced orientations, a molecular relaxation process takes place which is determined by the rate of heat transfer. The bead-and-spring macromolecular theory was used to calculate root mean end-to-end distances of macromolecules in the various flow fields, as well as the relaxation process.

INTRODUCTION

The injection molding process consists of filling a cold-walled cavity with hot polymeric melt. The properties of injection-molded objects are anisotropic and nonhomogeneous. This, in amorphous polymers, is a result of orientation of the macromolecules induced by the flow process. Some of the orientation is lost by a relaxation process prior to solidification in the mold; therefore, anisotropy is reduced when polymer relaxation times are short and solidification time is long. Yet, economy demands the shortest time cycle within the quality requirements, thus rendering the detailed understanding of the orientation distribution, its mechanism of formation, and its dependence on material properties and operating conditions, an important industrial problem. The orientation distribution is rather complex, because every fluid particle in the finished object has a different temperature and deformation history.

Two main experimental techniques have been used to investigate orientation in injection molding: birefringence measurements and shrinkage at elevated temperature of microtomed samples cut from the product. The former technique is limited to transparent products yet it is not restricted to the finished product, but can be applied also during the filling process. The latter technique, though limited to the finished product, is applicable to any polymer.

* Permanent address: Department of Chemical Engineering, Technion, Haifa, Israel.

Optical birefringence studies of injection-molded objects were done by several investigators.[1–5] Ballman et al.[1,2] related the observed birefringence to molecular orientation[2] and correlated its magnitude to both mechanical properties and operating conditions. They also reviewed the earlier literature dealing with this subject. They suggest that shear flow is the main source of orientation and that molecular relaxation after cessation of flow is a process which reduces the orientation. Mean birefringence as well as birefringence profiles across the sections were reported. These profiles were of varying complexity with one or more maxima. Wales et al.[5] also relate the birefringence to shear flow and relate its magnitude to shear stress at the wall during the mold-filling process. This relationship appeared to be independent of temperature and of the macroscopic rate of deformation.

A study of orientation by measuring shrinkage of microtomed samples heated above the softening range of the polymer was reported by Menges and Wubken,[6] who also refer to earlier reports on this technique. The authors measured the shrinkage distribution of amorphous polystyrene as a function of processing conditions, both in the direction of flow and perpendicular to it. Their measurements indicate a complex orientation distribution with one or more maxima. This is in qualitative agreement with Jackson and Ballman's[1] results.

In Figure 1, some of the data given by Menges and Wubken[6] for amorphous polystyrene are reproduced. In the direction of flow, shrinkage was maximum at the surface, decreased with distance from the surface, passed through a maximum, and dropped to zero at the center. Transverse shrinkage was also maximum at the wall and zero at the center, but no secondary maxima were observed.

Increase in melt temperature reduced shrinkage, whereas increase in injection speed increased shrinkage at the surface and changed the distribution (see Fig. 1). These are some of their conclusions, and they are in agreement with earlier reports.[2]

The authors assume a priori that the shrinkage of the samples is directly related to molecular orientation, which is caused by the flow during the mold-filling process. They suggest that orientation at the surface originates in the advancing melt front during the filling process, and this would also be the source of the transverse orientation. The rest of the orientation is due to shear flow which develops behind the front. The secondary maximum in shrinkage is suggested to be related to a maximum in shear rate which must exist somewhere between the solidified layer on the wall and the center. Coupled with the orientation process, a competing molecular relaxation process takes place.

It should be noted at this point that the relationship between shrinkage, or recoverable strain, and the original flow field might be rather complicated. Lodge[7] predicted that if an elastic liquid is subjected to steady uniform shear flow, a rather complex strain recovery in all three spatial directions is to be expected and that the magnitude of the strain recovery

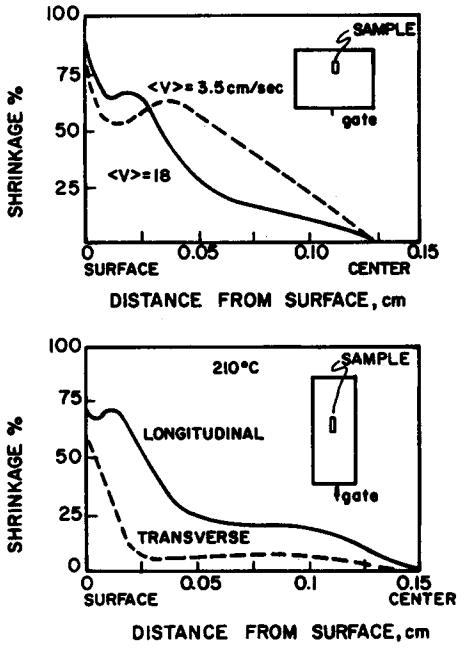

Fig. 1. Shrinkage distribution of injection-molded amorphous polystyrene, measured by Menges and Wubken.[6]

is a function of the applied shear. Later, Pollet[8] verified these predictions experimentally with poly(vinyl chloride) samples.

The findings and suggestion reported by Menges and Wubken[6] are important in pointing out that there are two major sources of orientation in injection molding: the advancing front and the shear flow behind it. Previously, orientation was attributed only to shear flow.

This might also explain some of the observations made in studying the detailed morphologic structure of injection-molded crystalline polymers.[9] Here, just as with amorphous polymers, a highly oriented "skin" was observed on the surface. Below the "skin" a "shear nucleated spherulitic intermediate layer" was found, and then a typically spherulitic core.

The purpose of this work is to suggest a model which combines flow patterns with molecular theories and the heat transport problem and which predicts semiquantitatively the observed complex orientation patterns. First, however, because of the intimate connection between the flow patterns and the orientation problem, the former will be analyzed in some detail.

FLOW PATTERNS DURING MOLD FILLING

The Advancing Front

The salient feature of the mold-filling process is the existence of an advancing front. The flow problem in advancing fronts was dealt with by

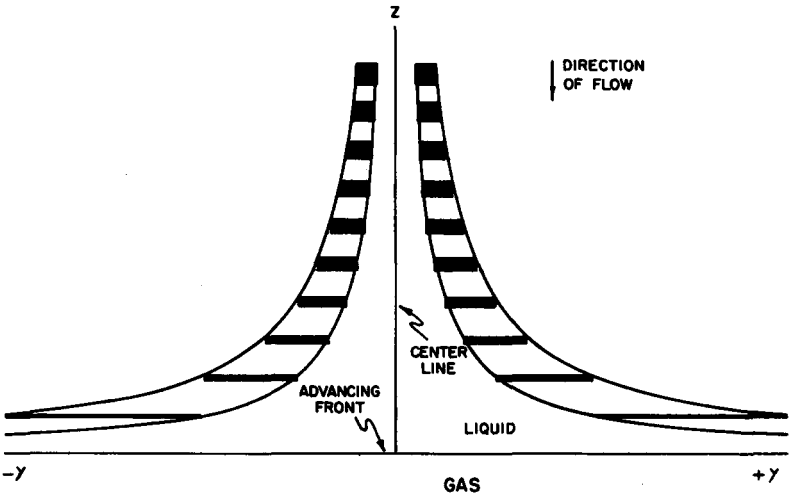

Fig. 2. Schematic representation of the flow pattern in the central portion of the advancing front between two parallel plates. The coordinate system moves in the z-direction with the front velocity. Shaded areas denote the stretching deformation the fluid particles experience.

investigators who were interested in problems associated with flow of one fluid replacing another, e.g., in a capillary. In such cases, interesting problems arise relating to the interface. Let's assume a particular case, with the interface moving at constant velocity. In such a situation, it is convenient to adopt a Lagrangian point of view, where the coordinate system (the viewer) will be moving with the same velocity as the interface, i.e., the mean velocity.

Rose[10] treated this problem qualitatively and, for describing the flow kinematics, appropriately designated the term "fountain effect." The flow, in his description, is such that "fluid particles in the central space decelerate as they approach the slower moving interface and acquire a radial component of velocity as they spill toward the wall region." Correspondingly, a "reverse fountain effect" takes place in the fluid ahead of the interface.

Similar observations were made by Swartz et al.[11] who visualized the phenomenon experimentally by injecting dye into the fluid, and they describe their observations as follows: "The index proceeds forward by rolling away from the tube wall and inward toward its center axis at the rear, while rolling outward from its center axis and on to the tube wall in front. There was no apparent sliding of liquid along the tube wall."

These and other points of interest related to the problem, in particular, the movement of the contact line over the solid surface, which apparently violates the "no slip" condition, was treated in detail in an interesting paper by Huh and Scriven.[12] Their calculations indicate that for a flat fluid interface moving steadily over a flat solid, rather complex velocity fields

may develop, which, among other things, depends on contact angle and viscosity ratio. However, these difficulties are probably less important in dealing with an advancing front of highly viscous polymer melt into an air-filled cavity. Bhattacharji and Savic[13] dealt with the problem of viscous pipe flow driven by a fluid piston. A phenomenon close to the "reverse fountain effect" was observed experimentally and predicted theoretically.

The above discussion consisted of a mixture of experimental observations, intuitive insight of the flow pattern, and some quantitative calculations. All this prior work points toward the possibility that the kinematics in the advancing front could be approximated by an incompressible stagnation potential flow which is identical to steady elongational flow. Although this assumption appears to be an oversimplification of the kinematics in the whole advancing front, it should be realized that the main interest (regarding orientation) focuses around the central portion of this front, where it appears to be a reasonable approximation. Figure 2 depicts this central portion of the front with the origin of the coordinate system at the center of the front and moving with it. The z-coordinate points upstream, and the y-coordinate points toward the wall, which is at distance B from the center. The velocity profile for a two dimensional flow (e.g., flow into a wide slit) is given approximately by

$$v_x = 0 \tag{1}$$

$$v_y = \bar{\kappa} y \tag{2}$$

$$v_z = -\bar{\kappa} z \tag{3}$$

where $\bar{\kappa}$ is the rate of elongation, whereas for a three-dimensional flow it is

$$v_x = \frac{\bar{\kappa}}{2} x \tag{4}$$

$$v_y = \frac{\bar{\kappa}}{2} y \tag{5}$$

$$v_z = -\bar{\kappa} z. \tag{6}$$

Referring to Figure 2, the velocity pattern described in eqs. (1) to (3) implies that a rectangular fluid particle while moving toward the front will decelerate in the axial direction, will accelerate in the perpendicular direction, and during this process will be stretched in the latter (y) direction at a constant rate. The rectangular shape will be maintained during this process, with the initial Δz_0 reduced to $\Delta z_0 e^{-\bar{\kappa} t}$ and the initial Δy_0 stretched to $\Delta y_0 e^{\bar{\kappa} t}$, where t is the time during which the particle is followed.

In such a steady elongational flow, macromolecules are stretched and oriented in the y-direction. The degree of orientation, as shown later, depends on the rate of elongation, which is hard to predict quantitatively without further experimental work. It will be assumed here for an order-of-magnitude calculation that at a distance of $2B$ upstream of the front a

fully developed shear flow exists. Therefore, the rate of elongation is given by the following expression:

$$-\bar{\kappa} = \frac{v_{\max} - \langle v \rangle}{2B} \tag{7}$$

where $v_{\max}$ is the maximum velocity of the fully developed flow and $\langle v \rangle$ is the mean velocity. Further assuming (as a first-order approximation) a power law model fluid in isothermal flow,

$$v_{\max} = \frac{2n + 1}{n + 1} \langle v \rangle \tag{8}$$

where n is the power law exponent. By substituting eq. (8) into eq. (7), the rate of elongation becomes

$$-\bar{\kappa} = \frac{n}{2(n + 1)B} \langle v \rangle. \tag{9}$$

Now, the suggested flow pattern implies an elongational orientation perpendicular to the main flow (i.e., in the y-direction), whereas experimental observation reveals orientation in the direction of the flow. This apparent discrepancy can be reconciled by recalling the actual shape of the advancing front, which is close to semicircular.[10] Thus, the fluid particles will actually follow the free surface in a curved path until they reach the wall, as shown in Figure 3. At this point, the orientation of the fluid particles and of the macromolecules is parallel to the wall. If the flow is two-dimensional, i.e., wide slit, the orientation will be exclusively in the flow direction; whereas if the front moves into a rectangular cross-sectioned cavity which is not very wide, orientation both in the direction of flow and transverse to it (i.e., z- and x-directions) would be expected. If the cross section is square or circular, the longitudinal and transverse orientations should be very close to each other. Experimental evidence supporting these predictions is indicated by the data reported by Menges and Wubken.[6]

The curved shape of the advancing front, however, also causes some difficulties to the assumed model. First, the exact shape of the surface is unknown, although assuming a semicircular shape may not be a very bad assumption. Next, the assumed kinematics in the front imply no shear deformation, which violates the theorem that for a curved free surface, irrotational flow cannot satisfy the boundary conditions.[14] This implies that in the front close to the curved surface, a shear flow must exist to balance surface tension. These forces will also determine the shape of the surface. Yet it is assumed here that such a shear flow will have an insignificant effect on the orientation problem.

The fluid particles which will hit the cold wall will immediately solidify, thus freezing in the orientation induced by the elongational flow they have experienced. The magnitude of this orientation, as pointed out earlier, depends on the rate of elongation. Equation (9) indicates, therefore, that an increase in injection speed and a decrease in cavity thickness will result

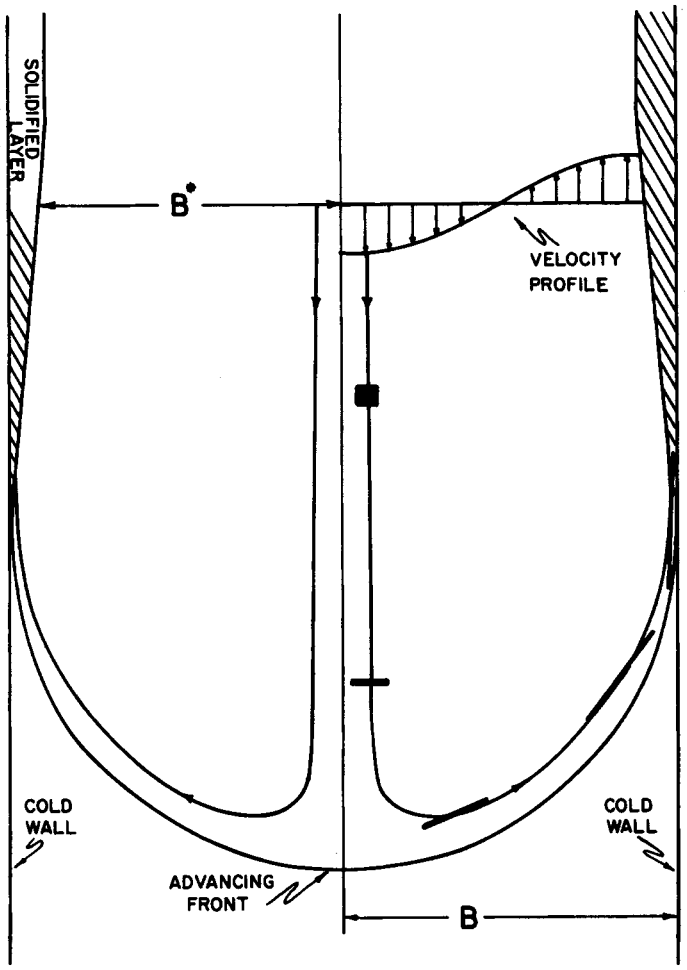

Fig. 3. Schematic representation of the flow pattern in the advancing front between two parallel plates. The shaded areas denote the stretching and orientation of a fluid particle. Due to the curved nature of the advancing front, the orientation of the particle arriving to the cold walls will be parallel to the wall. The velocity profile is relative to a moving coordinate system.

in an increase in orientation. Both effects were observed experimentally,[2,6] thus lending further qualitative support to the proposed model.

The Shear Flow Behind the Front

At some point upstream from the advancing front, a velocity profile exists which is probably quite close to that of a fully developed flow (at the instantaneous, local flow rate). In the previous section, this point was arbitrarily assumed to be at distance $2B$ upstream from the front. The flow at this point (and at all other upstream points all the way to the gate) takes place between two thin solidified layers of polymer. The expected shape of the velocity profile is shown in Figure 3 (as viewed from

the moving coordinate system). The shear rate is zero at the solid interface, goes through a maximum, and drops to zero at the center. Shear flow, just as elongational flow, induces molecular orientation; therefore, the detailed structure of the velocity profile would be needed. Although considerable attention was given to various aspects of this problem in the literature,[15,16,17] exact solution of this problem is difficult, because it is a heat transfer problem with phase transition coupled with non-Newtonian nonisothermal flow. The specific problem of flow into injection molds was also treated in several interesting papers by Harry and Parrot,[18] Kamal and Kenig,[19] and Berger and Gogos.[20] Unfortunately, the complexity of the problem inevitably leads to rather tedious numerical solutions. A series of velocity profiles calculated by Gogos,[21] at a fixed location in the mold at various times, is shown in Figure 4. The profiles indicate a quick buildup of a solidified layer, a maximum shear rate at some distance in between the interface and the center line, and a similarity in the shape of the velocity profiles at various times.

In view of the fact that the purpose of this work was limited to suggest a model which describes the possible mechanism of orientation formation, it will suffice to have a velocity profile which by an adjusrable parameter is capable of reproducing the more accurately calculated profile. Such a profile is given in eq. (10):

$$\frac{v_z}{\langle v \rangle} = \frac{(J+1)(J+2)(J+3)}{2}\left[\frac{\left(1-\frac{y}{B^*}\right)^{J+1}}{J+1} - \frac{\left(1-\frac{y}{B^*}\right)^{J+2}}{J+2}\right] \tag{10}$$

where J is the adjustable parameter and B^* is the distance from the center line to the solidifying interface (see Fig. 3). Equation (10) simplifies to isothermal Newtonian flow for $J = 0$.

The shear rate distribution is

$$\kappa = \frac{dv_z}{dy} = -\frac{(J+1)(J+2)(J+3)}{2}\frac{\langle v \rangle}{B^*}\frac{y}{B^*}\left(1-\frac{y}{B^*}\right)^J \tag{11}$$

which, of course, gives a zero shear rate at $y = 0$ and $y = B^*$.

The shear rate attains a maximum value at

$$y = \frac{B^*}{1+J}. \tag{12}$$

Therefore, by simply adjusting the parameter J, the location of maximum shear rate can be set equal to the location obtained from a more accurate calculation. Velocity profiles, calculated via eq. (10) for various J values, are shown in Figure 5.

The velocity profile (and the shear rate distribution which determines the orientation distribution) at a fixed location varies in time. Fortunately, this variation is not too large, because, as pointed out by Barrie,[22] the thickness of the solidified layer increases with the cube root of time.

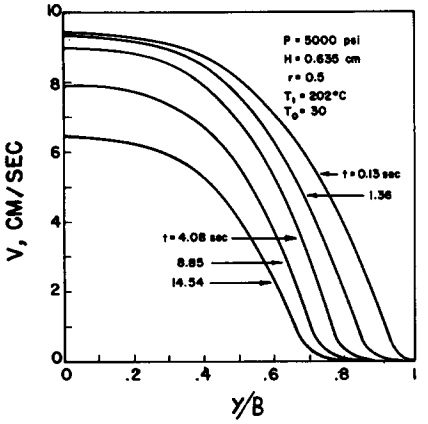

Fig. 4. Velocity profiles in radial flow in a disc-shaped mold at a fixed location and various times, calculated by Gogos.[21]

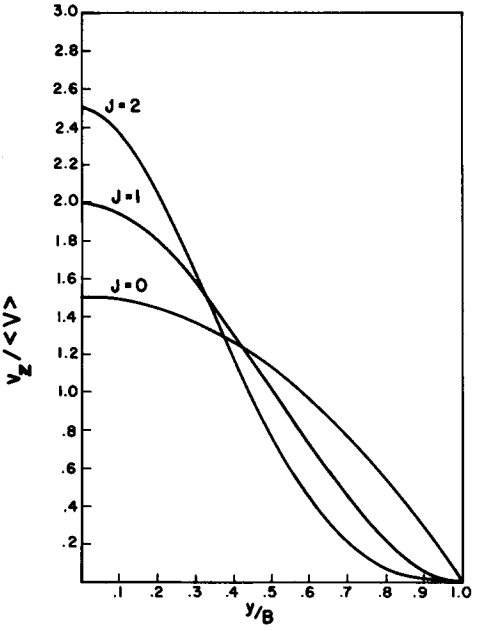

Fig. 5. Velocity profiles calculated from eq. (10) with J as parameter.

Therefore, the thickness of the solidified layer is surprisingly uniform throughout substantial portion of the mold.

THE ORIENTATION MODEL

Qualitative

It is suggested in this work that the orientation in the surface layer ("skin") is induced by steady elongational flow in the advancing front, as

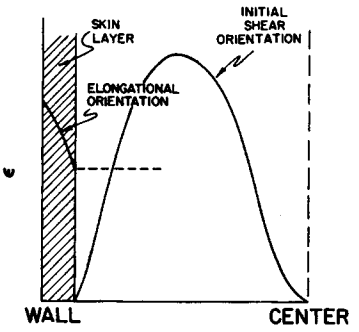

Fig. 6. Schematic representation of elongational and shear orientation upon cessation of flow.

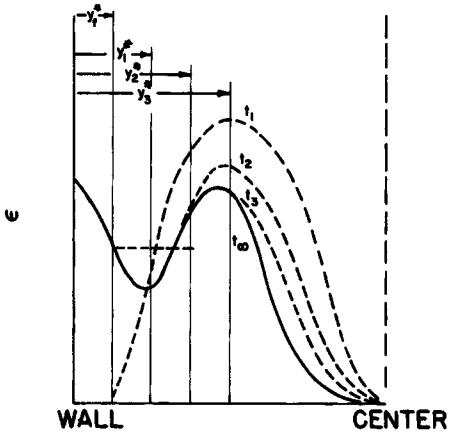

Fig. 7. Schematic representation of orientation distribution at various times: y_f^* is the thickness of solidified layer upon cessation of flow; y_1^* is the thickness after time t_1, etc. Solid curve indicates final frozen orientation.

given in eqs. (1) to (6), and with an elongational rate given in eq. (9). A layer of uniformly oriented molecules is placed on the cold surface by the advancing front. The fluid contacting the cold surface solidifies instantaneously; thus, the maximum orientation induced in the front is retained in it. The source of the "skin" layer is the central region of the flow where shear rates are very low; therefore, it can be assumed that there is no prior deformation history of this layer except the elongational flow in the front. Deeper layers do not solidify immediately; therefore, they have a chance to relax some of the orientation. The time for relaxation is determined by the distance from the surface, and it can be calculated by estimating the time needed for the moving solid melt interface to reach that layer. This mechanism explains qualitatively the experimentally observed orientation distribution in the skin layer as shown in Figures 1 and 6.

In modeling the shear rate-induced orientation, it will be assumed that the skin layer is thin and that the velocity profile between the thin frozen

layers, at any fixed location, is maintained until the abrupt cessation of flow when the mold is filled. The shear rate distribution, just prior to cessation of flow, as given in eq. (11), determines the initial shear oriented distribution as shown in Figure 6. Upon the cessation of flow, relaxation of molecular orientation starts. The time of relaxation of any fluid particle, just as in the skin layer, is the time needed for the moving solid–melt interface to reach that particle. This process is depicted schematically in Figure 7. The resulting orientation distribution is therefore identical in shape to the experimentally observed distributions as shown in Figure 1.

Quantitative

In order to convert the above described qualitative model into a quantitative, or at least semiquantitative, model, molecular flow theories are needed which would predict the behavior of macromolecules in elongational and shear flows. Fortunately, such theories were worked out in considerable detail.[23,24] Which particular theory among the ones available is the most suitable for this model is yet to be determined. In this work, a particular case of the bead-spring model derived by Bird et al.[23,25] was adopted with two beads connected with a Hookean spring. This model provides molecular end-to-end distances, for both elongational and shear flow, in simple analytical forms.

Although the theory was developed for dilute polymer solutions, it was shown by Lodge[26] that similar theories yield constitutive equations of the same form to those obtained by the network model and differ only in the interpretation of the constant coefficients. Furthermore, dilute solution theories have been applied to concentrated solutions with considerable success. One can speculate that in concentrated solutions and melts, the "bead-and-spring" concept actually represents clumps of molecules. If this is indeed the case, the application of this and similar dilute solution models to concentrated solutions and melts may turn out to be useful. Yet, in doing so, great care should be exercized in interpreting the results.

For elongational flow described by eqs. (1) to (3), the end-to-end distance is given by the following equation (see Appendix):

$$\langle r^2 \rangle = \frac{3kT}{H} + \frac{8kT}{H} \frac{\lambda^2 \bar{\kappa}^2}{(1 - 2\lambda\bar{\kappa})(1 + 2\lambda\bar{\kappa})} \tag{13}$$

where k is the Boltzmann constant, T is the temperature, H is the spring constant, and λ is a relaxation time. λ is a material property and can be calculated from molecular parameters or evaluated from the viscosity η as follows:

$$\eta = n_0 kT\lambda \tag{14}$$

where n_0 is the number of macromolecular chains per unit volume.

The first term on the right-hand side in eq. (13) expresses the equilibrium end-to-end distance $\langle r^2 \rangle_e$ under no-flow conditions or complete relaxation. According to this expression, for any particular material, the rate of elonga-

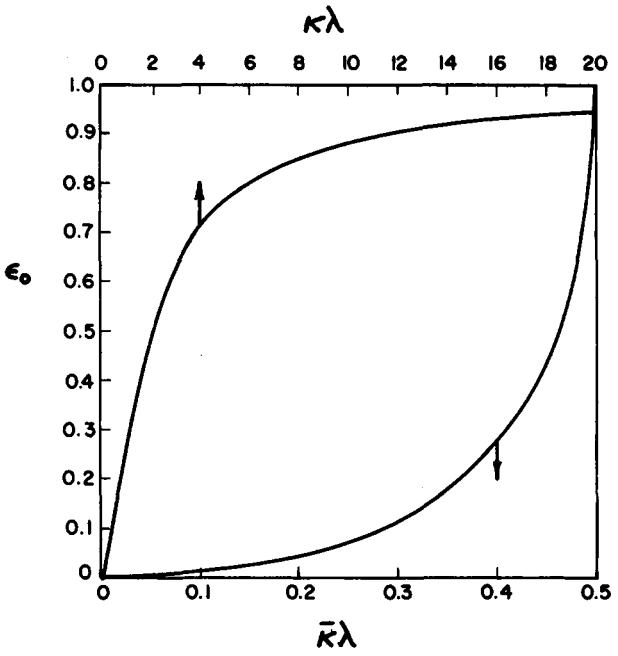

Fig. 8. Elongational and shear orientation calculated respectively from eqs. (15) and (22).

tion uniquely determines the end-to-end distance in flow. The difficulty, however, is that it predicts an infinite stretching of the macromolecule at finite rates of elongation (at $|\lambda\bar{\kappa}| = 0.5$). This shortcoming is the consequence of assuming a Hookean spring, and it could be eliminated by either assuming a nonlinear spring or preferably a FENE (Finitely Extendible Nonlinear Elastic) dumbbell.[27,28] These models, however, lead to complicated expressions which have to be evaluated numerically and are therefore avoided in this work.

Equation (13) can be rearranged to express the relative change in root mean end-to-end distance as follows:

$$\epsilon_0 = \frac{\langle r^2\rangle^{1/2} - \langle r^2\rangle_e^{1/2}}{\langle r^2\rangle^{1/2}} = 1 - \frac{1}{\sqrt{1 + \dfrac{8\lambda^2\bar{\kappa}^2}{3(1 - 2\lambda\bar{\kappa})(1 + 2\lambda\bar{\kappa})}}}. \qquad (15)$$

Equation (15) indicates that for $\bar{\kappa} = 0$ (i.e., no-flow condition), $\epsilon_0 = 0$, while for $|\lambda\bar{\kappa}| = 0.5$, $\epsilon_0 = 1$.

Now, ϵ_0 would represent shrinkage of elongated samples, as measured by Menges and Wubken,[6] provided it can be assumed that the relative change in end-to-end distance on a molecular scale is identical to macroscopic changes in that direction, i.e., the affine deformation assumption holds. Although this point requires further careful analysis, the expression given in eq. (15) probably does give an order-of-magnitude estimate of the shrink-

age as well as first-order estimates as to changes in orientation with operating variables. Figure 8 shows a plot of ϵ_0 versus $\lambda\dot{\kappa}$.

The mean square end-to-end distance will be assumed to relax exponentially in time upon cessation of flow just as normal stresses do[23]:

$$\frac{\langle r^2\rangle_t - \langle r^2\rangle_e}{\langle r^2\rangle_0 - \langle r^2\rangle_e} = e^{-t/\lambda} \tag{16}$$

where $\langle r^2\rangle_t$ is the mean square end-to-end distance at time t and $\langle r^2\rangle_0$ is the distance at time zero. By substituting eq. (16) into eq. (15), the following relationship between shrinkage at any time t, ϵ_t, and initial shrinkage ϵ_0 is obtained:

$$\epsilon_t = \frac{\langle r^2\rangle_t^{1/2} - \langle r^2\rangle_e^{1/2}}{\langle r^2\rangle_t^{1/2}} = 1 - \frac{1}{\sqrt{1 + \left[\left(\frac{1}{1-\epsilon_0}\right)^2 - 1\right]e^{-t/\lambda}}}. \tag{17}$$

The time t in eq. (17) corresponds to the time elapsed until the particular layer under consideration freezes. Therefore, by solving the heat transfer problem of the solidifying skin layer, a relationship is obtained between time and distance from the surface, y^*. As pointed out earlier, numerical solution can provide this relationship, however, considering the approximation made so far, it will be assumed that the Neumann problem[29] with constant physical properties will suffice in accuracy. The time according to this solution is related to thickness of solidified layer as follows:

$$y^* = At^{1/2} \tag{18}$$

where A is to be evaluated from the following expression:

$$\frac{(T_m - T_w)k_s e^{-A^2\beta^2/4\alpha_s}}{\sqrt{\pi\alpha_s}\, erf\,(A\beta/2\sqrt{\alpha_s})} - \frac{(T_0 - T_m)k_m e^{-A^2/4\alpha_m}}{\sqrt{\pi\alpha_m}\, erfc\,(A/2\sqrt{\alpha_m})} - \frac{\lambda_f \rho_s A\beta}{2} = 0. \tag{19}$$

Equation (19) indicates that A depends primarily on the melt and wall temperature, and, of course, on physical properties. A good estimate of A can be obtained by substituting in eq. (18) B for y^* and the mold cooling time for t.

Finally, by substituting eq. (18) into eq. (17), an expression for the shrinkage as a function of distance for the skin layer is obtained:

$$\epsilon_t = 1 - \frac{1}{\sqrt{1 + \left[\left(\frac{1}{1-\epsilon_0}\right)^2 - 1\right]e^{-y^{*2}/A^2\lambda}}}. \tag{20}$$

The derivation for the shrinkage orientation distribution in the shear flow follows along similar lines. The square end-to-end distance for steady shear flow is given[25] by the following equation:

$$\langle r^2\rangle = \frac{3kT}{H} + \frac{2kT}{H}\lambda^2\dot{\kappa}^2. \tag{21}$$

Equation (21) can be rearranged to give the following expression for the relative change in root mean end-to-end distance:

$$\epsilon_0' = \frac{\langle r^2\rangle^{1/2} - \langle r^2\rangle_e^{1/2}}{\langle r_2\rangle^{1/2}} = 1 - \frac{1}{\sqrt{1 + \frac{2}{3}\lambda^2\kappa^2}}. \tag{22}$$

As in elongational flow, so also in shear flow the orientation is a unique function of shear rate κ. In Figure 8, ϵ_0' is plotted versus $\lambda\kappa$; but, unlike in elongational flow, here the problem of infinite stretching at finite shear rates does not appear.

The initial orientation distribution upon cessation of flow can be obtained by substituting κ values obtained from eq. (11) into eq. (22). It should be noted, however, that by doing this substitution, eq. (21) is assumed to be locally valid in a nonuniform shear field.

Now, further assuming an exponential relaxation as given in eq. (16), the relative change in root mean end-to-end distance, or shrinkage, can be obtained as a function of time:

$$\epsilon_t' = 1 - \frac{1}{\sqrt{1 + \left[\left(\frac{1}{1 - \epsilon_0'}\right)^2 - 1\right] e^{-t'/\lambda}}}. \tag{23}$$

The time t' is the time available to a fluid layer for relaxation, and it corresponds to the time needed for the solid–melt interface to move from the point it was at the cessation of flow (the thickness of the skin layer) to the layer under consideration. This is given approximately by the following expression:

$$t' = t - t_f = \frac{y^{*2} - y_f^{*2}}{A^2} \tag{24}$$

where y_f^* is the thickness of the skin layer corresponding to time t_f.

Finally, by substituting eq. (24) into eq. (23), the following expression is obtained for shrinkage due to shear orientation as a function of distance from the surface:

$$\epsilon_t' = 1 - \frac{1}{\sqrt{1 + \left[\left(\frac{1}{1 - \epsilon_0'}\right)^2 - 1\right] e^{-(y^{*2} - y_f^{*2})/A^2\lambda}}}. \tag{25}$$

NUMERICAL EXAMPLE

A sample calculation was carried out for one of the data points reported by Menges and Wubken[6] and shown on Figure 1. The purpose of the calculation is not to prove the validity of the model—for this purpose the model in its present form is too crude and the information on the experiment insufficient—but merely to justify its basic structure.

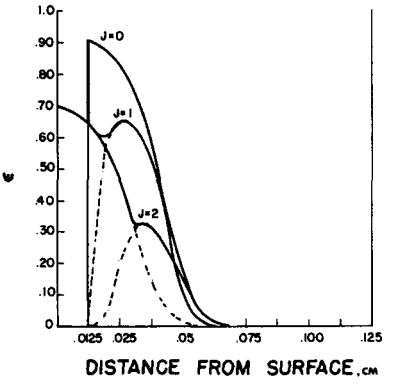

Fig. 9. Shrinkage distribution calculated for the following conditions: $\langle v \rangle = 3.5$ cm/sec; $B = 0.125$ cm; $\epsilon_0 = 0.7$; $n = 1/3$; cooling time = 5 sec, with J as a parameter.

The mean injection speed in one of the experiments is $\langle v \rangle = 3.5$ cm/sec, and the plate separation is $2B = 0.25$ cm. Under these conditions, the maximum surface orientation was $\epsilon_0 = 0.70$. The thickness of the skin layer appears to be approximately 0.0125 cm, and the shrinkage distribution is shown in Figure 1.

The rate of elongation $\bar{\kappa}$ can be calculated from eq. (9) by assuming $n = 1/3$. Thus, $\bar{\kappa} = 3.5$ sec^{-1}. Now, from eq. (15), with the experimentally measured surface orientation $\epsilon_0 = 0.7$, the relaxation time can be obtained, $\lambda = 0.14$ sec. This value would fall within the range of λ as estimated from eq. (14). Furthermore, the time of relaxation should be not much different in order of magnitude from the cycle time. The resulting λ is not unreasonable from this point of view.

The value of A was estimated from eq. (18) by assuming a cooling time of 5 sec, i.e., $A \cong B/\sqrt{5}$. With this information, the shrinkage profile was calculated for a series of J values with eqs. (20) and (25). The results are shown in Figure 9. These indicate that the relaxation time in the skin layer is too high, whereas that in the shear zone is too low. This is the reason also for the high sensitivity of the results to the parameter J. There are two reasons for this: first, it would be reasonable to assume that the relaxation time in a non-Newtonian fluid will be larger upon cessation of flow, while in the model a single relaxation time is used; but, more importantly, during the cooling time the temperature of every fluid layer decreases gradually prior to freezing. The relaxation time should therefore increase. This effect was excluded from the model. Finally, the cooling time, which was arbitrarily assumed, also affects the results. By including these effects, more orientation will be predicted in the central zone and the sensitivity to J will decrease.

The preliminary results indicate that J should be in the range $0 < J < 1$. From eq. (12), this implies that the maximum shear rate should be at $B/2 < y < B$. The calculated velocity profiles in Figure 4 seem to support this conclusion.

It would be easy to vary some of the parameters of the model and adjust a calculated curve to the experimental one, but this is not the purpose of this sample problem. The results shown in Figure 9 do indicate, however, that the proposed model contains the essential features which would allow one to predict the rather complex orientation distribution. Furthermore, the brief analysis of the results indicates that by including in the model some obviously missing effects, agreement with experiments would improve.

DISCUSSION

The experimental data on orientation in injection moldings, reviewed briefly in this work, indicate a rather complex distribution of orientation which depends in a sensitive way on the polymer, the mold, and the operating conditions.

The model which is proposed in this work, extending previous suggestions in the literature, incorporates all these effects—the suggested flow and heat transfer mechanisms in the mold are coupled with macromolecular theories to result, at this stage, in a semiquantitative model. Although this model includes numerous assumptions, it sheds some light on the source and nature of orientation in injection moldings. Thus, the steady elongational flow, which is suggested to occur in the advancing front, explains the high values and direction of orientation in the skin layer. It also suggests that the shape of the flow cross section determines whether this orientation will be uniaxial or biaxial. The molecular theory indicates that the magnitude of the orientation should be determined by the relaxation time, which is very sensitive to temperature, and the rate of elongation. This dependence leads to the conclusion, supported by experimental observation, that orientation increases with increasing injection speed and decreases with plate separation and increasing temperature. The sensitivity to both these variables should decrease as orientation level increases. The molecular relaxation process, coupled with the heat transfer, explains the drop in orientation with distance from the surface. Recent measurements by Gurnee[31] of orientation distribution in thin-walled polystyrene cups reveal a relatively low surface orientation value. This finding might indicate a further aspect of the orientation mechanism in the advancing front. It is possible that under certain conditions molecular orientation due to elongational flow is not fully developed. In either case, nonisothermal effects due to viscous dissipation might also play a significant role. Neither effects were considered in this work. The shear flow behind the front is the source of the molecular orientation in the core of the sample. The orientation distribution induced by this flow, coupled with relaxation, leads to prediction consistent to experimental observations.

The model admittedly is no more than semiquantitative, yet it includes hopefully some of the essential features of the orientation mechanisms; and it is felt that by a process of eliminating the numerous simplifying assumptions (many of which were introduced for the sole purpose to keep it

as simple as possible), it can be converted into a quantitative model. This elimination process, however, should be preceded by, or done in parallel with, a considerable amount of additional experimental work.

Appendix

End-to-End Distance of Macromolecules in Elongational Flow

The flow field is described in eqs. (1) to (3). Rewriting the velocity components in coordinates x_1, x_2, and x_3, we get

$$v_1 = \bar{\kappa} x_1 \tag{1-A}$$

$$v_2 = -\bar{\kappa} x_2 \tag{2-A}$$

$$v_3 = 0. \tag{3-A}$$

For this flow we therefore get for ∇v

$$\nabla v = \begin{bmatrix} 1 & 0 & 0 \\ 0 & -1 & 0 \\ 0 & 0 & 0 \end{bmatrix} \bar{\kappa} \tag{4-A}$$

and for the rate of deformation tensor

$$\dot{\gamma} = \begin{pmatrix} 1 & 0 & 0 \\ 0 & -1 & 0 \\ 0 & 0 & 0 \end{pmatrix} 2\bar{\kappa}. \tag{5-A}$$

The mean square end-to-end distance for a Rouse model[30] is

$$\langle (\underline{r}_N - \underline{r}_1)^2 \rangle = \frac{3(N-1)kT}{H} - \frac{1}{N_0 H} t_r \tau_p \tag{6-A}$$

where N is the number of beads and τ_p is the polymeric contribution to the stress tensor τ.

The stress tensor τ_p is, for the Rouse model,[30]

$$\tau_p = -\int_{-\infty}^{t} G_1(t-t')\gamma_{[1]}(t')dt' \tag{7-A}$$

with

$$G_1(t-t') = n_0 kT \sum_{m=1}^{N-1} e^{-\frac{t-t'}{\lambda_m}} \tag{8-A}$$

and

$$\gamma_{[1]ij} = \sum_m \sum_n \frac{\partial x_i}{\partial x_{m'}} \frac{\partial x_j}{\partial x_{n'}} \dot{\gamma}_{mn}. \tag{9-A}$$

in order to perform all the substitutions, the "displacement" functions $x_i = x_i(x_j', t, t')$ are needed. These are obtained as follows:

$$v_1 = \bar{\kappa} x_1 = \frac{d}{dt} x_1 \tag{10-A}$$

$$v_2 = -\bar{\kappa} x_2 = \frac{d}{dt} x_2. \tag{11-A}$$

Therefore,

$$x_1 = x_1' e^{\bar{\kappa}(t-t')} \tag{12-A}$$

and

$$x_2 = x_2' e^{-\bar{\kappa}(t-t')}. \tag{13-A}$$

Then,

$$\gamma_{[1]} = \begin{bmatrix} 2\bar{\kappa}e^{2\bar{\kappa}(t-t')} & 0 & 0 \\ 0 & -2\bar{\kappa}e^{-2\kappa(t-t')} & 0 \\ 0 & 0 & 0 \end{bmatrix} \tag{14-A}$$

and

$$\tau_p = -2n_0kT\bar{\kappa}\sum_{m=1}^{N-1}\int_{-\infty}^{t}\begin{bmatrix} e^{\left(2\bar{\kappa}-\frac{1}{\lambda_m}\right)(t-t')} & 0 & 0 \\ 0 & -e^{-\left(2\bar{\kappa}+\frac{1}{\lambda_m}\right)(t-t')} & 0 \\ 0 & 0 & 0 \end{bmatrix} dt' \tag{15-A}$$

Finally, we get for $tr\tau_p$ the following expression:

$$tr\tau_p = -2n_0kT\bar{\kappa}\sum_{m=1}^{N-1}\int_{-\infty}^{t}\left(e^{\left(2\bar{\kappa}-\frac{1}{\lambda_m}\right)(t-t')} - e^{-\left(2\bar{\kappa}+\frac{1}{\lambda_m}\right)(t-t')}\right)dt'$$

$$= 8n_0kT\bar{\kappa}^2\sum_{m=1}^{N-1}\frac{1}{\left(2\bar{\kappa}-\frac{1}{\lambda_m}\right)\left(2\bar{\kappa}+\frac{1}{\lambda_m}\right)} \tag{16-A}$$

Hence,

$$\langle(\underline{r}_N - \underline{r}_1)^2\rangle = \frac{3(N-1)kT}{H}\left[1 - \frac{8}{3}\frac{\bar{\kappa}^2}{N-1}\sum_{m=1}^{N-1}\frac{\lambda_m^2}{(2\lambda_m\bar{\kappa}-1)(2\lambda_m\bar{\kappa}+1)}\right]. \tag{17-A}$$

Finally, for a two-bead spring model, the mean end-to-end distance is

$$\langle r^2\rangle = \frac{3kT}{H} + \frac{8kT}{H}\frac{\lambda^2\bar{\kappa}^2}{(1-2\lambda\bar{\kappa})(1+2\lambda\bar{\kappa})}. \tag{18-A}$$

Nomenclature

A	heat transfer variable defined in eq. (19), cm/sec$^{1/2}$
B	half the separation between two parallel plates (half-thickness of injection-molded object), cm
B^*	distance between center line to the solidifying interface, cm
H	spring constant, dyne/molecule·cm
J	parameter in velocity profile
k	Boltzmann constant, erg/molecule·°K
$k_s k_m$	thermal conductivities of solid and melt, cal/sec·°K·cm
n	power law parameter
n_0	number of macromolecules per unit volume, molecules/cm^3
$\langle r^2\rangle$	mean square end-to-end distance of macromolecules, cm^2
$\langle r^2\rangle_t$	mean square end-to-end distance of macromolecules at time t, cm^2
$\langle r^2\rangle_e$	equilibrium mean square end-to-end distance of macromolecules, cm^2
t	time, sec
t_f	time for a skin layer of thickness y_f^* to develop, sec
t'	$t - t_f$, sec
T	temperature, °K
T_m	melting point, °K
T_0	temperature of in-flowing melt, °K

T_w wall temperature, °K
v_i velocity component in i-direction, cm/sec
v_{max} maximum velocity along the center line, cm/sec
$\langle v \rangle$ mean velocity, cm/sec
x rectangular coordinate, cm
y rectangular coordinate, cm
z rectangular coordinate, cm
α_s, α_m thermal diffusivities of solid and melt, cm²/sec
β ρ_m/ρ_s
ϵ_0 relative change in root mean end-to-end distance in elongational flow, defined in eq. (15)
ϵ_0' relative change in root mean end-to-end distance in shear flow, defined in eq. 22
η viscosity function, dyne·sec/cm²
κ rate of shear, sec^{-1}
$\bar{\kappa}$ rate of elongation, sec^{-1}
λ relaxation time, sec
λ_f heat of fusion, cal/g
ρ_s, ρ_m densities of solid and melt, g/cm³

It is a pleasure to acknowledge the help the author has received from Professor R. B. Bird in several discussions and in providing the derivation in the Appendix. He would also like to thank Professor A. S. Lodge for his comments on a draft of this paper; Professors L. E. Scriven (University of Minnesota) and M. W. Johnson, Jr., for their suggestions; Professor C. G. Gogos (Stevens Institute of Technology) for providing the data in Figure 4; Dr. R. A. Daane from the Beloit Corporation for his assistance; and the Graduate School of the University of Wisconsin and the Beloit Corporation for financial aid.

References

1. G. B. Jackson and R. L. Ballman, *SPE J.*, **16**, 1147 (1960).
2. R. L. Ballman and H. L. Toor, *Mod. Plast.*, **38**, 113 (1960).
3. W. Woebcken, *Kunststoffe*, **51**, 547 (1961).
4. E. F. T. White, B. M. Murphy, and R. N. Haward, *J. Polym. Sci.*, **B7**, 157 (1969).
5. J. L. S. Wales, I. J. van Leeuwen, and R. vander Vijgh, *Polym. Eng. Sci.*, **12**, 358 (1972).
6. G. Menges and G. Wubken, Annual Technical Conference of the Soc. of Plastics Eng. Preprints, Montreal, Canada, 1973, p. 519.
7. A. S. Lodge, in *Rheology of Elastomers*, P. Mason and N. Wookey, Eds., Pergamon Press, London, 1958, p. 70.
8. W. F. O. Pollet, *Rheol. Acta*, **1**, 257 (1958).
9. M. R. Kantz, H. D. Newman, and F. H. Stigale, *J. Appl. Polym. Sci.*, **16**, 1249 (1972).
10. W. Rose, *Nature*, **191**, 242 (1961).
11. A. M. Swartz, C. A. Rader, and E. Huey, *Contact Angles Wettability and Adhesion*, R. F. Gould, Ed., American Chemical Society, Washington, D.C., 1964, p. 250.
12. C. Huh, and L. E. Scriven, *J. Colloid Interfac. Sci.*, **35**, 85 (1971).
13. S. Bhattacharji and P. Savic, *Proc. Heat Transfer Fluid Mech. Inst.*, 1965, p. 248.
14. L. D. Landau and E. M. Lifshitz, in *Course of Theoretical Physics*, Vol. 6, Pergamon Press, Oxford, 1959, p. 233.

15. J. E. Porter, *Trans. Inst. Chem. Eng.*, **49**, 1 (1971).
16. S. G. Bankoff, in *Advances in Chemical Engineering,*" Academic Press, New York, 1964, p. 75.
17. R. D. Zerble and J. E. Sunderland, *J. Heat Transfer*, **90**, 185 (1968).
18. D. H. Harry, and R. G. Parrot, *Polym. Eng. Sci.*, **10**, 209 (1970).
19. M. R. Kamal and S. Kenig, *ibid.*, **12**, 294 (1972).
20. J. L. Berger and C. G. Gogos, *ibid.*, **13**, 102 (1973).
21. C. G. Gogos, private communication.
22. I. T. Barrie, *Plast. Polym.*, **38**, 47 (1970).
23. R. B. Bird, H. R. Warner, Jr., and D. C. Evans, *Advan. Polym. Sci.*, **8**, 1 (1971).
24. A. S. Lodge, *Elastic Liquids*, Academic Press, London and New York, 1964.
25. R. B. Bird, M. W. Johnson, Jr., and J. F. Stevenson, Proc. of the Fifth Congr. on Rheology, Vol. 4, S. Onogi, Ed. University of Tokyo, 1970, p. 159.
26. A. S. Lodge, and Y. J. Wu, *Rheol. Acta*, **10**, 539 (1971).
27. J. F. Stevenson and R. B. Bird, *Trans. Soc. Rheol.*, **15**, 135 (1971).
28. H. R. Warner, Jr., *Ind. Eng. Chem.*, Fundam., **11**, 379 (1972).
29. E. R. G. Eckert and R. M. Drake, Jr., *Analysis of Heat and Mass Transfer*, McGraw Hill, New York, 1972.
30. R. B. Bird, *Macromolecular Hydrodynamics*, Rheology Research Center Report 14, University of Wisconsin, 1973.
31. E. F. Gurnee, submitted for publication to *J. Appl. Polym. Sci.*

Received November 6, 1973
Revised November 30, 1973